Appl Microbiol Biotechnol (2015) 99:9577–9589
DOI 10.1007/s00253-015-6710-2

Increased riboflavin production by manipulation of inosine 5′-monophosphate dehydrogenase in *Ashbya gossypii*

Rubén M. Buey[1] · **Rodrigo Ledesma-Amaro** · **Mónica Balsera**[2] · **José María de Pereda**[3] · **José Luis Revuelta**[1]

Received: 17 March 2015 / Revised: 15 May 2015 / Accepted: 19 May 2015 / Published online: 7 July 2015

Abstract Guanine nucleotides are the precursors of essential biomolecules including nucleic acids and vitamins such as riboflavin. The enzyme inosine-5′-monophosphate dehydrogenase (IMPDH) catalyzes the ratelimiting step in the guanine nucleotide de novo biosynthetic pathway and plays a key role in controlling the cellular nucleotide pools. Thus, IMPDH is an important metabolic bottleneck in the guanine nucleotide synthesis, susceptible of manipulation by means of metabolic engineering approaches. Herein, we report the functional and structural characterization of the IMPDH enzyme from the industrial fungus *Ashbya gossypii*. Our data show that the overexpression of the IMPDH gene increases the metabolic flux through the guanine pathway and ultimately enhances 40 % riboflavin production with respect to the wild type. Also, IMPDH disruption results in a 100-fold increase of inosine excretion to the culture media. Our results contribute to the developing metabolic engineering toolbox aiming at improving the production of metabolites with biotechnological interest in *A. gossypii*.

Keywords *Ashbya gossypii* · Metabolic engineering · Riboflavin · Inosine 5′-monophosphate dehydrogenase

Electronic supplementary material The online version of this article (doi:10.1007/s00253-015-6710-2) contains supplementary material, which is available to authorized users.

✉ Rubén M. Buey
ruben.martinez@usal.es

✉ José Luis Revuelta
revuelta@usal.es

[1] Metabolic Engineering Group, Departamento de Microbiología y Genética, Universidad de Salamanca, Edificio Departamental, Campus Miguel de Unamuno, 37007 Salamanca, Spain

[2] Department Abiotic Stress, Instituto de Recursos Naturales y Agrobiología, Consejo Superior de Investigaciones Científicas, C/ Cordel de Merinas 40-52, 37008 Salamanca, Spain

[3] Instituto de Biología Celular y Molecular del Cáncer, Consejo Superior de Investigaciones Científicas, Universidad de Salamanca, Campus Miguel de Unamuno, 37007 Salamanca, Spain

Introduction

Guanine nucleotides are essential for cell viability. They are not only precursors of nucleic acids but they also represent the energy source for translation and microtubule polymerization and are implied in signal transduction, angiogenesis (Chong et al. 2006), and axon guidance (Long et al. 2006), among many other cellular functions. From a biotechnological point of view, guanine nucleotides are very significant as they are the metabolic precursors of a variety of metabolites with biotechnological interest, such as tetrahydrobiopterin (Gross and Levi 1992), guanosine 5′-monophosphate (GMP) flavor enhancer (Ledesma-Amaro et al. 2015), folates (vitamin B9; (Cossins and Chen 1997)), or riboflavin (vitamin B2; (Bacher et al. 2000)).

Industrial riboflavin production is, in fact, one of the most representative examples illustrating the importance of microbial metabolic engineering to substitute chemical synthesis by a much more convenient microbial biosynthesis: contrary to the common practice several decades ago, currently, microbial fermentation yields essentially the whole commercial riboflavin production in the world, estimated in 8000 t/year (Park et al. 2011). More than half of this riboflavin is produced by fermentation of the filamentous fungus *Ashbya gossypii*, which is considered a paradigm of the sustainable and environmentally friendly "white biotechnology" (Vandamme 1992; Stahmann et al. 2000; Park et al. 2011; Kato and Park 2012).

As a natural riboflavin overproducer, the guanine nucleotide metabolism has an obvious relevance, given that guanosine 5′-triphosphate (GTP) is the riboflavin-limiting precursor (Stahmann et al. 2000). The guanine nucleotides are synthesized in two different ways: in the de novo pathway, the purine ring system is assembled in a step-wise manner from biosynthetic precursors of carbohydrate and amino acid metabolism and from ammonia and carbon dioxide (Zalkin and Dixon 1992). On the other hand, the salvage pathways recycle preformed nucleobases, nucleosides, and nucleotides (Murray 1971).

Within the de novo purine nucleotide (adenine and guanine derivatives) biosynthetic route, guanosine 5′-monophosphate (IMP) is the first compound in the pathway to have a completely formed purine ring system that is synthesized on a pre-existing ribose-phosphate scaffold through a complex pathway that involves ten sequential enzymatic reactions. IMP is the common precursor of both adenine and guanine nucleotides (Fig. 1a). IMP dehydrogenase (IMPDH) catalyzes the oxidation of IMP to xanthosine 5′monophosphate (XMP) with the concomitant reduction of (nicotinamide-adenine dinucleotide) NAD^+ to NADH (Fig. 1b). XMP is subsequently converted to GMP in a reaction catalyzed by the enzyme GMP synthetase (GMPS), and GMP is further converted into GTP in successive steps (Fig. 1a). Riboflavin is subsequently synthesized from GTP and ribulose 5-phosphate in a pathway controlled by the *RIB* genes (Bacher et al. 1996; Revuelta et al. 1998).

GTP availability is known to be the limiting factor for riboflavin production, as demonstrated by the fact that exogenous supplementation of GTP synthetic precursors improves its production (Stahmann et al. 2000). Therefore, an exhaustive characterization of the enzymes involved in GTP biosynthesis is necessary in order to settle the basis for metabolic and protein engineering approaches aiming at improving production levels in this fungus. Indeed, we have previously reported that an enhancement of the metabolic flux through the purine pathway, induced by the manipulation of the enzymes phosphoribosyl pyrophosphate (PRPP) amidotransferase and PRPP synthetase, results in a significant increase in riboflavin production by *A. gossypii* (Jiménez et al. 2005, 2008), as a consequence of augmented GTP availability. Aiming at further redirecting the metabolic flux towards riboflavin synthesis, in this study, we focused on the guanine nucleotide pathway after the IMP metabolic knot (Fig. 1a).

Within the guanine nucleotide pathway, the reaction catalyzed by IMPDH takes place at the branch point between the guanine and adenine nucleotide de novo biosynthetic pathways (Fig. 1a) and it does not only represent the rate-limiting step in guanine nucleotide biosynthesis but also plays a fundamental role in the central metabolism as a key regulator of the cellular nucleotide pools (Allison and Eugui 2000). In fact, human IMPDHs have been extensively studied since several decades, given their interest as antitumor targets: its

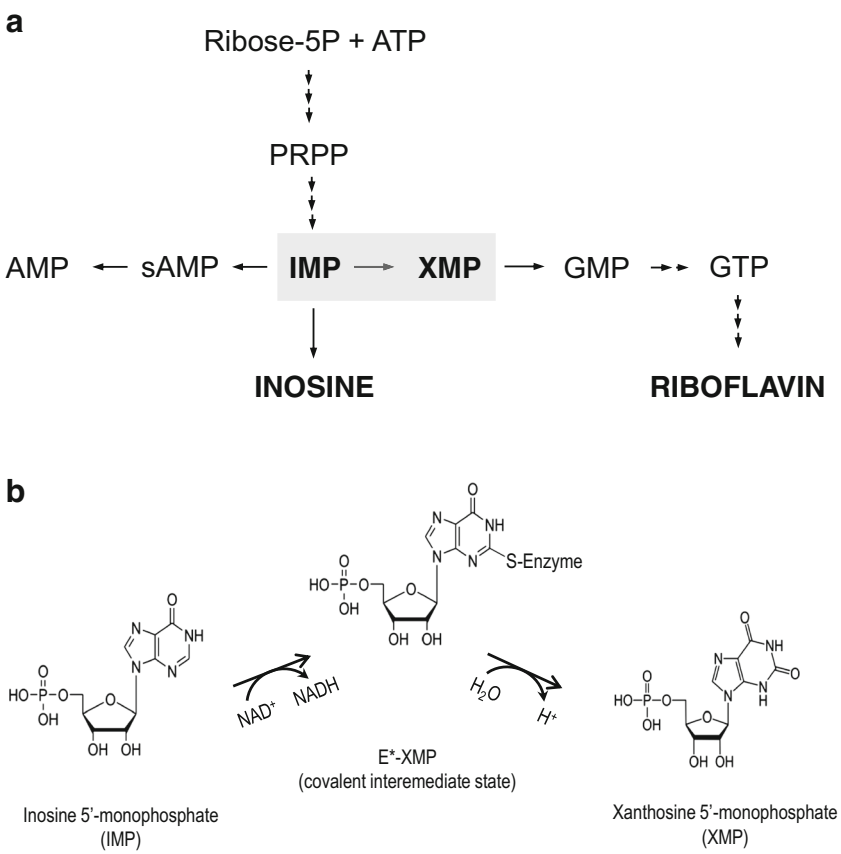

Fig. 1 Schematic—simplified—representation of the de novo purine pathway (**a**) and the reaction catalyzed by the enzyme IMP dehydrogenase (**b**)

pharmacological inhibition depletes the guanine pool, limiting the large nucleotide requirements necessary to support the enhanced growth of tumor cells (Braun-Sand and Peetz 2010). Furthermore, IMPDH has also emerged as a major target for antiparasitic (Umejiego et al. 2008), antiviral (Nair and Shu 2007), antibacterial (Hedstrom et al. 2011), and immunosuppressive therapies (Ratcliffe 2006). As a consequence, IMPDHs from different organisms have been biochemically and structurally characterized, focusing on their therapeutic value (for review, see (Hedstrom 2009)).

In the present work, we report the functional, biochemical, and structural characterization of the enzyme IMPDH from *A. gossypii* (AgIMPDH). We show that the IMP dehydrogenase activity is encoded by a single gene in its genome which is essential for growth in media lacking guanine. We describe the enzyme kinetics in vitro as well as the high-resolution crystal structures of the catalytic domain of AgIMPDH bound to the substrate IMP and the product XMP. We further show that the genetic manipulation of this enzyme significantly influences the metabolic flux through the guanine nucleotide pathway and, consequently, the production of riboflavin. Our results do not only identify a central bottleneck for riboflavin production but also settle the functional and structural basis for future metabolic and protein engineering approaches in *A. gossypii*, aiming at improving the production of GTP-derived metabolites with biotechnological and industrial interest.

Materials and methods

Strains, media, and techniques for *A. gossypii* culture

The *A. gossypii* ATCC 10895 was considered as the wild-type strain in this work. The different strains used were grown at 28 °C with orbital shaking at 150 rpm in rich MA2 medium (Forster et al. 1999). When required, a concentration of 250 μg/mL of geneticin (G418; Sigma-Aldrich St. Louis, MO) was used. *A gossypii* transformation, sporulation, spore isolation, and nucleic acid isolation were performed as described elsewhere (Jiménez et al. 2005, 2008; Ledesma-Amaro et al. 2014b; Wendland et al. 2000).

AgIMPDH gene disruption and overexpression

The *ΔIMPDH* strain (AgIMPDH disrupted), was obtained following methodologies previously described (Jiménez et al. 2005, 2008; Ledesma-Amaro et al. 2014b; Wendland et al. 2000). Briefly, a replacement DNA cassette containing the *kanMX4* selection module including the geneticin resistance ($G418^r$) and flanked by specific homology regions was transformed into spores of the wild-type strain. Homokaryotic $G418^r$ transformants were obtained after sporulation and clonal selection of the primary heterokaryotic transformants.

The P_{GPD}-*IMPDH* strain (AgIMPDH overexpressed) was obtained as follows: the AgIMPDH ORF was inserted into a DNA cassette comprising a selection module for geneticin resistance, a recombination module for stable integration into the *STE12* locus, and an overexpression module based on the *A. gossypii* glycerol 3-phosphate dehydrogenase promoter (P_{GPD}) and terminator sequences, which have been reported to provide constitutive and high expression transcription levels (Ledesma-Amaro et al. 2014a, b). This DNA cassette was transformed into spores of the *ΔIMPDH* strain and the transformants, prototroph for guanine in contrast to the parental strain, selected in minimal media. As before, homokaryotic transformants were obtained after sporulation and clonal selection of the primary heterokaryotic transformants. All strains were checked for correct integrations by PCR amplification and DNA sequencing.

DNA integration into the *STE12* locus has been extensively tested in our lab, and no significant metabolic alterations have been detected upon *STE12* disruption (our unpublished results). Production of riboflavin, inosine, and guanine for the *ΔSTE12* deletion mutant is shown in Table S2 in Supplementary Information. Additionally, it has been reported that deletion of *STE12* increases sporulation (Wendland et al. 2011; Wasserstrom et al. 2013), which represents a convenient characteristic for strain manipulation in the lab.

Protein purification

AgIMPDH ORF was inserted into a modified version of the pET15b vector (Alonso-García et al. 2009). The Bateman domain was removed from the wild-type sequence by PCR splicing to construct the mutant enzyme AgIMPDH-ΔBateman (Fig. 2a). All DNA constructs were corroborated by DNA sequencing. Proteins were expressed in *Escherichia coli* strain BL21-DE3 (Agilent Technologies, St. Clara, CA) and purified by nickel-chelating affinity chromatography according to standard protocols. The His_8 tag present at the N terminus of the fusion proteins was cleaved by digestion with tobacco etch virus protease (His_6-tagged as well), and was removed by a second nickel-affinity chromatography. The cleaved protein was then injected into a HiPrep Sephacryl S-300 16/60 HR size-exclusion chromatography column (GE Healthcare, Little Chalfont, UK) equilibrated in buffer 20 mM Tris-HCl, 150 mM KCl, 0.5 mM Tris(2-carboxyethyl)phosphine (TCEP), pH 8.0. Fractions containing AgIMPDH protein were pooled, concentrated in 10-kDa cutoff centrifugal filters, flash-frozen into liquid nitrogen, and stored at −80 °C until used. The enzymes remained 100 % active after thawing.

IMPDH activity assay and enzyme kinetics

IMPDH activity was assayed at 28 °C using 96-well micro titer plates by monitoring the reduction of NAD^+ to NADH

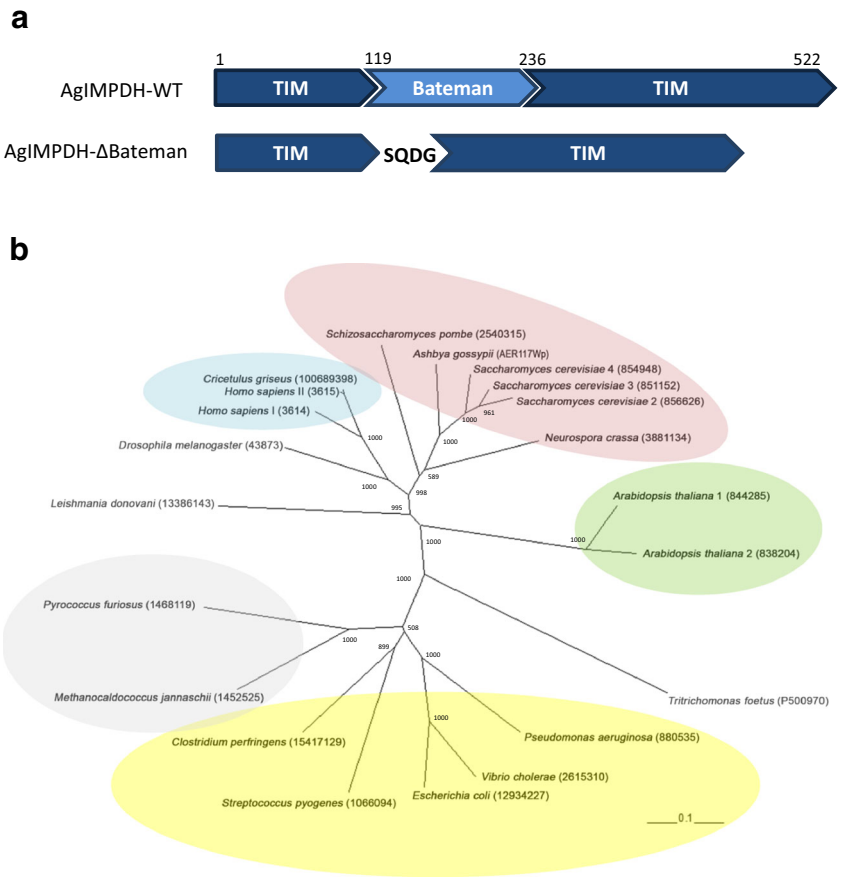

Fig. 2 **a** Schematic representation of the protein domain organization of the IMPDH wild-type and ΔBateman enzymes in *A. gossypii*. **b** Phylogram of representative members of the IMPDH protein family showing the optimal unrooted phylogenetic tree obtained by ClustalX (Thompson et al. 2002). Bacteria are colored in *orange*, archaea in *gray*, mammals in *blue*, fungi in *red*, and plants in *green*. Gene IDs according to NCBI are shown in parentheses. Bootstrap values are shown for each branch. Branch lengths are proportional to evolutionary distances. The figure has been generated with TreeView (Page 1996)

and the subsequent increase in absorbance at 340 nm. Reaction buffer contained 100 mM Tris-HCl, 100 mM KCl, 2 mM dithiothreitol (DTT), pH 8.0. Final enzyme concentration was adjusted to 20 μg/mL, and NAD^+ concentration was fixed at 0.5 mM while varying IMP from 39 μM to 5 mM and vice versa. In our experimental conditions, V_0 values could not be reliably determined for product (NADH) concentrations below 20 μM, which is the estimated sensitivity limit of our assay. Experimental data (V_0) were fitted by non-linear regression to standard Michaelis-Menten enzyme kinetics equations using the GraphPad Prism software (GraphPad Software, La Jolla, CA) to derive the values of K_M, K_{cat}, K_i, and V_{max}.

Crystallization and structure determination of the catalytic domain of AgIMPDH

Crystals of the mutant enzyme AgIMPDH-ΔBateman were grown at room temperature using vapor diffusion methods by mixing a protein solution at 23 mg/mL in 10 mM Tris-HCl, 100 mM KCl, 0.25 mM TCEP, pH 8.0 with an equal volume of mother liquor consisting of 0.1 M HEPES, pH 7.5, 40 % Polyethylene Glycol 300 (PEG-300; *v*/*v*), 0.2 M NaCl. Crystals of AgIMPDH with IMP bound to the active site were obtained by vapor diffusion in mother liquor: 25 % (*v*/*v*) 1,2-propanediol, 0.1 M citrate-phosphate pH 4.2, 5 % (*w*/*v*) PEG-3000, 10 % (*v*/*v*) glycerol, after adding up to 5 mM XMP and 5 mM NAD^+ to a 23 mg/mL AgIMPDH-ΔBateman protein solution. Under identical conditions, using protein at 23 mg/mL plus 5 mM XMP, we obtained crystals of AgIMPDH-ΔBateman with a mixture of ~80 % of the covalent intermediate E-XMP* and ~20 % IMP bound to the active site.

Prior to data collection, crystals were cooled by direct immersion in liquid nitrogen. Data were collected at 100 K at the XALOC beamline (ALBA synchrotron; (Juanhuix et al. 2014)). Diffraction intensities were indexed and integrated by using the software XDS and scaled with XSCALE (Kabsch 2010).

A mixed search model for molecular replacement (Jaroszewski et al. 2011) was built by homology modeling using as template the crystal structure of the equivalent region (template PDB code: 4AVF). Data were then phased by molecular replacement using the program PHASER (McCoy et al. 2007) within the CCP4 suite (Potterton et al. 2003). The structures were iteratively refined by using the program phenix.refine within the PHENIX crystallographic software package (Adams et al. 2010), alternated with manual model building using COOT (Emsley et al. 2010). Simulated annealing (Cartesian coordinates) was used in the initial stages of refinement, while gradient-driven positional, individual

isotropic B-factor restrained and TLS refinement (Winn et al. 2001) were used in the last steps. 4XTI was refined against twinned data using a merohedral twinning operator h,-k,-l. Water molecules were placed into peaks over 3σ of $mf_{obs} - Df_{calc}$ maps and 1σ of $2mf_{obs} - Df_{calc}$ maps when reasonable H-bonding patterns were observed. All the models have excellent geometry with 98 % of the main chain torsion angles located in the favored regions of the Ramachandran plot and no outliers.

Protein data bank accession numbers

The atomic coordinates and structure factors of the apo and IMP and E-XMP* complex structures have been deposited in the Research Collaboratory for Structural Bioinformatics Protein Data Bank under ID codes 4XWU, 4XTD, and 4XTI, respectively.

Metabolite analysis

Extracellular nucleoside concentrations were determined from the mycelia contained in 5 mL of culture broth, which was harvested by filtration on a filter paper, dried overnight at 100 °C and weighted. The filtered media was passed through a 0.2-μm polyvinylidene difluoride (PVDF) membrane (Acrodisc® LC; Pall, Port Washington, NY) and injected into an AQUASIL C18 140 × 4.6 mm column (Thermo Scientific, Waltham, MA) connected to an HPLC (Compact LC 1120; Agilent Technologies, St. Clara, CA) and monitored by absorbance at 260 nm. Separation of nucleosides was achieved by using an isocratic flow of 100 mM potassium phosphate buffer, pH 5.5, 0.5 % acetonitrile. Quantification was carried out by using a calibration curve prepared with pure standards of inosine and guanosine (Sigma-Aldrich, St. Louis, MO). All analyses were performed using three biological replicates. Total (intra and extracellular) riboflavin production levels were measured using a spectrophotometric assay. Briefly, a volume of 1 M HCl was added to 1 mL of culture and incubated at 100 °C for 30 min. After cooling down the samples, the mycelium was lysed using 0.5-mm glass beads (Sigma-Aldrich, St. Louis, MO) and vigorous vortex. After centrifugation, the concentration of riboflavin in the supernatant was determined spectrophotometrically at 450 nm on a Varioskan microtiter plate reader (Thermo Scientific, Waltham, MA). The calibration curves were obtained using pure riboflavin (Sigma-Aldrich, St. Louis, MO) and processed in the same way as the samples.

Bioinformatic analysis

Sequence homology searches (blastp) were performed using the IMPDH protein sequence from *Saccharomyces cerevisiae* (ScIMD3, (Hyle et al. 2003)) as a template on the Ashbya Genome Database (Gattiker et al. 2007) and the non-redundant GenBank database (Benson et al. 2014). All the retrieved sequences were aligned with the ClustalX program (Larkin et al. 2007), visually inspected and manually corrected. The non-conserved regions of the alignment were removed using the software Gblocks (Castresana 2000), and the phylogenetic analysis was performed by using the neighbor joining method, as implemented in ClustalX (Thompson et al. 2002). Bootstrap values were inferred from 1000 replicates. The phylogenetic tree was displayed with TreeView (Page 1996).

Results

IMP dehydrogenase activity is encoded by a single gene in *A. gossypii*

Sequence homology searches identified *AER117W* in *A. gossypii* as the only gene encoding for the metabolic enzyme inosine-monophosphate dehydrogenase, in marked contrast with the four genes that are encoded in *S. cerevisiae*'s genome (Hyle et al. 2003), an organism evolutionarily closely related to *A. gossypii* (Dietrich et al. 2004). The *IMPDH* gene contains a 161-bp-long intron after the codon 151. Remarkably, only one of the four genes that encode for this activity in *S. cerevisiae* (*IMD4*) contains an intron, and this encodes for the protein with closest homology to AgIMPDH (78.2 % identity, Fig. S1 in the Supplementary Material), in accordance with the evolutionary hypothesis previously proposed for *A. gossypii* and *S. cerevisiae* (Dietrich et al. 2004).

Multiple sequence alignments (Fig. S1 in the Supplementary Material) and bootstrapped phylogenetic trees (Fig. 2b) of IMPDHs from different organisms clustered fungal IMPDHs close to the two human isoforms and far away from the bacterial IMPDHs (around 60 and 30 % sequence identity, respectively). These results are in accordance with the deep branching of the bacterial and eukaryotic forms of IMPDH that has been previously observed (Zhang et al. 1999a, b).

A protein sequence analysis revealed a nicotinamide adenine dinucleotide binding and IMPDH/GMP-reductase motifs, as well as two tandem cystathione β-synthase like motifs (CBS) that form the, so called, Bateman domain (Bateman 1997). Therefore, as it happens in most of the studied IMPD Hs (Hedstrom 2009), each monomer is composed of a catalytic and a regulatory domain (Fig. 2a). The latter domain, together with the N-terminal residues, constitutes the less conserved region in terms of sequence homology. Interestingly, the N-terminal residues form a helical structure that stabilizes the quaternary structure (see below) and seems to be unique for fungi (Fig. S1 in the Supplementary Material).

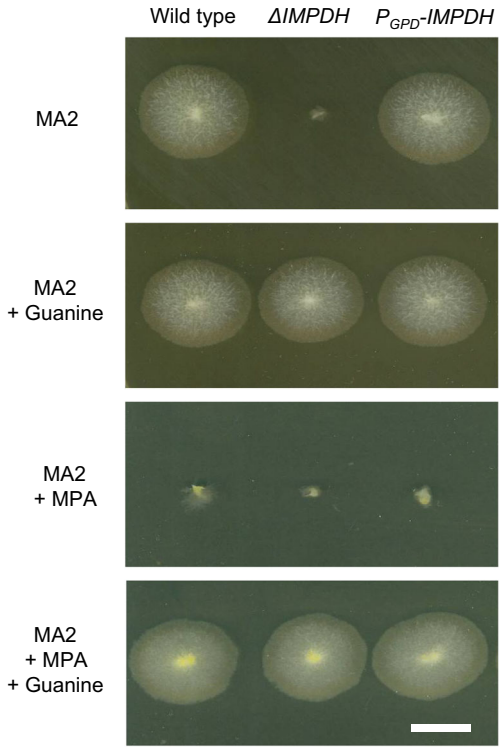

Fig. 3 Photographs of colonies of *A. gossypii* wild-type, *ΔIMPDH*, and P_{GPD}-*IMPDH* strains grown on solid MA2-rich medium with the specified additives (*MPA* mycophenolic acid) during 48 h at 28 °C. *Scale bar* = 1 cm

IMPDH is essential for the de novo GTP biosynthesis and cell growth

IMPDH catalyzes the first and rate-limiting step in the de novo GTP biosynthetic pathway. To corroborate that the gene *IMPDH* is the only one in *Ashbya*'s genome that encodes for IMPDH activity, we disrupted it in the widely used wild-type strain (ATCC10895). The resulting Δ*IMPDH* strain showed auxotrophy for guanine and was unable to grow in solid MA2-agar media (Fig. 3). Supplementation of the media with guanine restored growth (Fig. 3), through the action of the *salvage* pathway. Furthermore, the re-introduction, into the Δ*IMPDH* mutant strain, of the *IMPDH* gene at the *STE12* locus (Ledesma-Amaro et al. 2014a) under the control of the strong constitutive promoter of glyceraldehyde 3-phosphate dehydrogenase (P_{GPD}-*IMPDH*) also restored growth (Fig. 3), demonstrating that *AER117W* is the only responsible for the IMPDH activity in *A. gossypii*. In a similar way, as shown in Fig. 3, neither the wild-type nor the Δ*IMPDH* mutant strains were able to grow in the presence of the archetypal uncompetitive inhibitor mycophenolic acid (MPA). MPA is known to deplete the guanine pool in the cells, impeding growth (Allison and Eugui 2000). Therefore, after supplementation of the culture media with guanine, the phenotype was restored (Fig. 3), demonstrating that *A. gossypii* is able to overcome the loss of the IMPDH activity through the salvage pathway when guanine is present in the culture media.

Enzyme kinetics characterization of AgIMPDH in vitro

As stated above, *A. gossypii* is a natural riboflavin superproducer that must ensure a strong flux over the guanine nucleotide biosynthetic pathway to support a large availability of GTP, the limiting precursor of riboflavin. Thus, we aimed at characterizing the enzyme kinetics of IMPDH in vitro to decipher potential differences in catalytic efficiency with respect to other non-flavinogenic organisms, e.g., *S. cerevisiae*.

Recombinant full-length AgIMPDH (AgIMPDH-WT) was expressed in *E. coli* as a His_8 fusion protein and purified using conventional chromatographic methodologies. AgIMPDH was expressed at high levels in *E. coli*, yielding about 20–25 mg of >95 % pure protein per liter of culture. In order to facilitate crystallization (see below), we also produced, in a similar way, a mutant enzyme (AgIMPDH-ΔBateman) that only harbors the catalytic domain; the regulatory domain, spanning residues 120–235, has been substituted by residues SQDG. Both AgIMPDH-WT and AgIMPDH-ΔBateman enzymes are tetramers in solution, according to size-exclusion chromatography (Fig. S2A in the Supplementary Material).

Both enzymes (AgIMPDH-WT and AgIMPDH-ΔBateman) were assayed for IMP dehydrogenase activity by monitoring the appearance of NADH, as has been described elsewhere (Dobie et al. 2007). AgIMPDH shows optimal enzymatic activity in the presence of 100 mM potassium ions at pH 8.0, in common to many other IMPDHs (Hedstrom 2009). The enzyme kinetic analysis showed that the reaction obeys Michaelis-Menten's equation, with $K_{M,\ IMP}$ values in the same concentration range for AgIMPDH and AgIMPDH-ΔBateman (Fig. 4a, Table 1, and Fig. S2B in the Supplementary Material), demonstrating that the Bateman domain is dispensable for the enzymatic activity. The $K_{M,\ IMP}$ values are remarkably similar to those described for *S. cerevisiae* IMD3 (McPhillips et al. 2004; Jenks and Reines 2005). On the other hand, substrate inhibition was observed for NAD^+ (Fig. 4a) with K_i in the low millimolar range (Table 1). The enzyme shows a clear preference for NAD^+ over $NADP^+$, since it loses more than 95 % activity when using the latter as co-substrate (data not shown). Besides, attempts to measure the back conversion of XMP to IMP by AgIMPDH failed with either NADH or NADPH as hydride donor. Interestingly, the enzyme is competitively inhibited by the product XMP (Fig. 4b) with $K_i = 208.3 \pm 9.8$ μM and in an uncompetitive manner by mycophenolic acid (MPA; Fig. 4c) with $K_i = 32.07 \pm 3.2$ nM (Table 1).

High-resolution crystallographic structures of AgIMPDH

To further characterize AgIMPDH and to establish a reliable structural basis for eventual protein engineering experiments

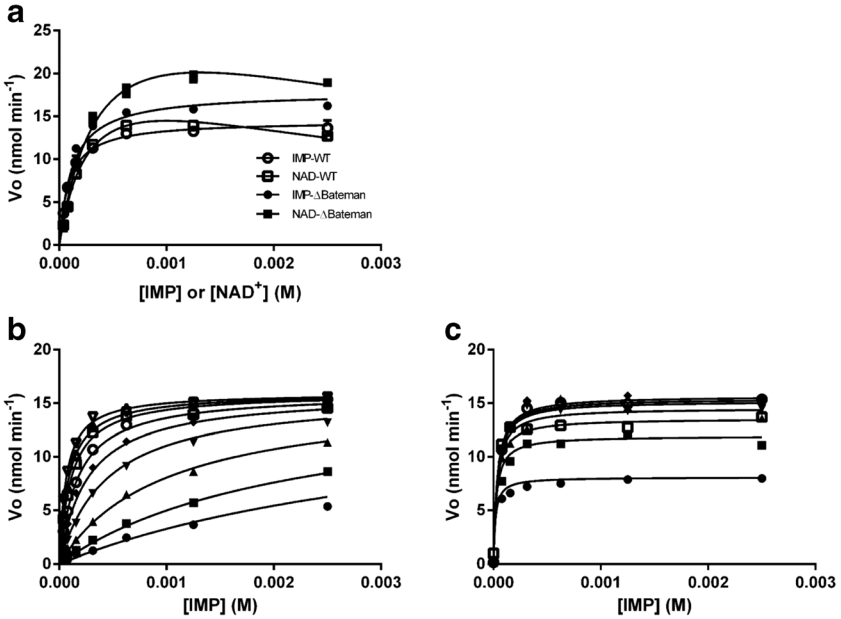

Fig. 4 Kinetic characterization of AgIMPDH. **a** AgIMPDH and AgIMPDH-ΔBateman kinetic constants, K_M, for IMP were calculated from the Michaelis-Menten equation by non-linear regression, while K_M and K_i for NAD^+ were estimated from a modified Michaelis-Menten equation to take into account substrate inhibition. *Error bars* represent the standard deviations of three independent measurements. **b** Competitive/feed-back inhibition of AgIMPDH by XMP. The plot represents the initial velocity versus IMP concentration in the presence of increasing concentrations of XMP (12.5, 7, 3, 1.25, 0.65, 0.35, 0.150, 0.075, and 0 mM). The K_M values change while V_{max} is constant, showing the typical pattern for competitive inhibition. Global fit $r^2 = 0.9964$. **c** Uncompetitive inhibition of AgIMPDH by mycophenolic acid. The plot represents the initial velocity versus IMP concentration in the presence of increasing concentrations of mycophenolic acid (30, 10, 5, 2.5, 1, 0.5, and 0 nM). Global fit $r^2 = 0.9687$

aiming at improving the enzyme efficiency and/or removing product inhibition, we sought to determine the high-resolution crystal structures of the apo-enzyme as well as in complex with the substrate IMP and the product XMP. Despite a considerable effort, we were unable to obtain protein crystals suitable for X-ray diffraction experiments for the full-length enzyme but we obtained crystals of the catalytically active AgIMPDH-ΔBateman enzyme; in accordance, previous reports have also described that the deletion of the regulatory domain facilitates crystallization (Hedstrom 2009). The crystal of apo-AgIMPDH- ΔBateman belongs to the space group I4 (Table S1 in the Supplementary Material) and contains a single monomer in the asymmetric unit with approximately 45 % solvent content. The monomer is related to the adjacent monomers in the crystal by a 4-fold symmetry axis that generates the tetramer found in solution (Fig. 5a). The tetramer is stabilized by inter-monomer contacts between adjacent subunits (Fig. 5a). Remarkably, the first N-terminal residues of AgIMPDH, including two short 3_{10} and an alpha helices, α0 (comprising residues 6–15), that are not present in bacterial and archaeal enzymes (Fig. S1 in the Supplementary Material), project from the catalytic domain and pack against helices α10 and α12 (according to *Bacillus anthracis* secondary structure nomenclature; (Makowska-Grzyska et al. 2012)) in the adjacent subunit of the tetramer, mostly through hydrophobic interactions (Fig. 5b). At the opposite site of the oblate that forms the tetramer, the C-terminal tails are packed together around the 4-fold axis (Fig. 5a).

The core of the catalytic domain comprises a $(\beta/\alpha)_8$ barrel which represents the typical triose-phosphate isomerase fold (TIM barrel, (Nagano et al. 2002)) and shows no significant conformational differences with the IMPDH structures from other organisms. In our final model, there is no interpretable electron density for neither the loop that contains the catalytic Cys334 (residues 330–339, loop β13-α11, according to *B. anthracis* nomenclature (Makowska-Grzyska et al. 2012)) nor the catalytic flap and finger domains (residues 401–455), suggesting that

Table 1 In vitro enzyme kinetic parameters of AgIMPDH

	$K_{M,\ IMP}$ (μM)	$K_{cat,\ IMP}$ (sec^{-1})	$K_{M,\ NAD}$ (μM)	$K_{i,\ NAD}$ (mM)	$K_{i,\ XMP}$ (μM)	$K_{i,\ MPA}$ (nM)
WT	90.2 ± 5.6	2.46 ± 0.04	279.8 ± 24.7	3.6 ± 0.5	208.3 ± 9.8	32.07 ± 3.2
ΔBateman	118.0 ± 13.1	3.06 ± 0.06	386.6 ± 38.7	4.5 ± 1.2	nd	nd

nd not determined

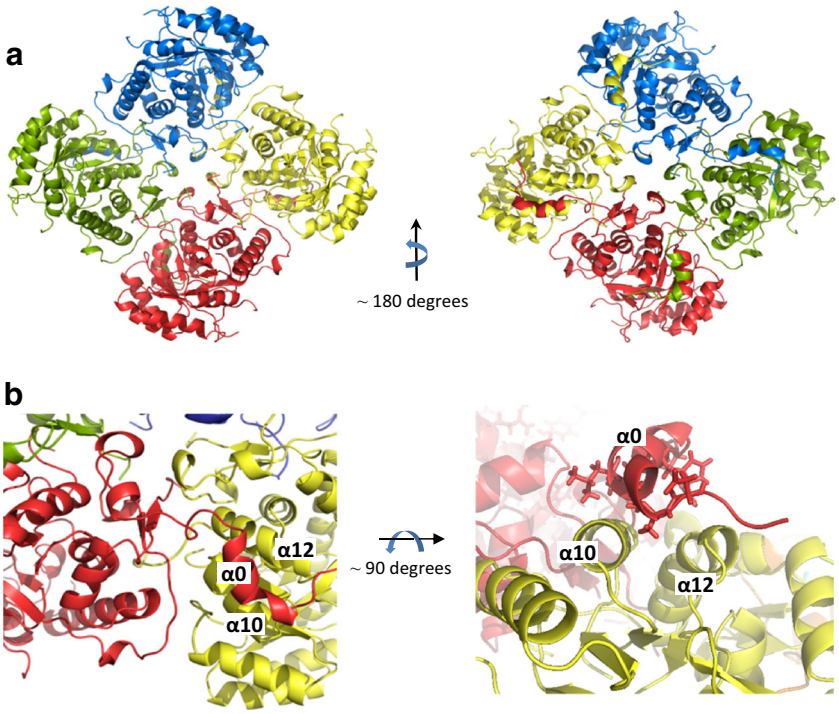

Fig. 5 Crystal structure of AgIMPDH-ΔBateman. **a** Ribbon representation of the tetrameric structure of AgIMPDH-ΔBateman with the 4-fold symmetry axis orthogonal to the paper plane. The four monomers are colored *blue*, *yellow*, *red*, and *green*. **b** Detailed view of the interface between monomers showing the packing of helix α0 (*red cartoon*) from one monomer with the helices α10 and α12 (*yellow cartoon*) of the adjacent monomer

they are rather flexible, especially in the absence of substrate or product, in common to previous reports of IMPDH structures from other organisms (Prosise et al. 2002; Hedstrom 2009; Morrow et al. 2012; Rao et al. 2013). There is also no electron density for the last 20 C-terminal residues, which also seem to be disordered in our crystals.

IMPDH catalyzes the oxidation of IMP to XMP with the concomitant reduction of NAD^+ to NADH. Therefore, in order to better characterize the active site of AgIMPDH for eventual protein engineering experiments, we aimed at determining the structures of AgIMPDH with either the substrate IMP or the product XMP bound to the active site. After multiple trials, we were able to obtain X-ray diffraction suitable crystals by co-crystallizing the AgIMPDH-ΔBateman protein after incubation either with 5 mM XMP plus 5 mM NAD^+ or with 5 mM XMP alone.

Both crystals belong to the space group P4 (Table S1 in the Supplementary Material) and contain two monomers in the asymmetric unit (AU) with approximately 44 % solvent content. The two monomers in the AU are related to their adjacent monomers in the crystal by a 4-fold symmetry axis that generates the tetramers found in solution, identical to those described above. In the structures for both complex structures, the finger domain, the loop containing the catalytic cysteine, and the C-terminal tail can be modeled within the electron density. These structures only lack 18–20 residues of the catalytic flap and a few residues from the loop containing the artificial SQDG linker that substitutes the Bateman domain in the AgIMPDH-ΔBateman mutant enzyme.

Surprisingly, despite an excess of XMP was added to the protein solution, careful inspection of the electronic density showed that the crystals contained either IMP or the covalent intermediate E-XMP* bound to the active site: the electron density for AgIMPDH-ΔBateman-XMP could be best modeled with a ~80–20 % mixture of E-XMP* and IMP for both monomers in the AU. On the other hand, AgIMPDH-ΔBateman-XMP-NAD^+ was modeled with a ~20–80 % mixture of IMP and E-XMP* for one monomer and 100 % IMP for the other monomer in the AU (Fig. S3 in the Supplementary Material). No clear electron density for NAD^+ was observed and, therefore, it was not modeled into the active site. This indicates that in the crystallization drop, the conditions within the crystal lattice forced over the time the back-conversion of the product into the substrate, a reaction that could not be reproduced in our solution experimental conditions (not shown).

The presence of these ligands into the active site does not induce significant reorganizations in the structure of the catalytic barrel (with respect to the apo-enzyme), and it is characterized by subtle and local changes in the structure of the loop comprising residues 366–373 (loop β14-α13) that reorganizes to accommodate the phosphate and ribose moieties of IMP. The catalytic Cys334 loop (loop β13-α11) and the C-terminal segment (β19 and α18) adopt a transition state-like structure (E-XMP*; Gan et al. 2003). In our crystals, the mobile flap presumably adopts a flexible, solvent-exposed, open conformation with no interpretable electron density. Although some disconnected blobs of electron density appear in the NAD^+ binding pocket, these are discontinuous and it was

not possible to model something inside with a minimum of reliability. This, in fact, might be an indication of a partial—low—occupation of the mobile flap into the NAD^+ site.

The conformations of XMP (in the E-XMP* structure) and IMP are essentially identical within the active site, with the purine ring system stabilized by hydrogen bonds with several protein backbone atoms: Met417 and Gly418 (in loop β17-α15) with atoms N7 and O6, respectively, and the side chain of Gln448 (in loop η3-β18) with atom N1. Additionally, Gly329 and Gly331 (in loop β13-α11) stabilize a water molecule that contacts the atom N3 (Fig. S4 in the Supplementary Material). The catalytic Cys334 (loop β13-α11) is either at 3.1 Å distance from the C2 atom of IMP, in a catalytically active position, or making a single C-S bond (distance 1.8 Å; (Trzhtsinskaya and Abramova 1991)) in E-XMP* (Fig. S3 in the Supplementary Material). In both complex structures (IMP and E-XMP*), the ribose moiety of the nucleotide is coordinated by the side chains of residues Ser74 (in loop β4-α1), Arg325 (in β13), and Asp367 (in β14) while the phosphate moiety is mainly coordinated by the backbone atoms of residues Ser332 (in loop β13-α11), Gly369 (in loop β14-α13), Gly390 and Gly391 (in helix α14), and the side chains of residues Ser332 (in loop β13-α11) and Tyr414 (in β17; Fig. 6 and Fig. S4 in the Supplementary Material).

Interestingly, electron density for a potassium ion appears in between the two monomers of the tetramer of the structure with IMP bound in the active site, coordinated by the oxygen backbone atoms of residues Gly329, Gly331, and Cys334 (in loop β13-α11) in one monomer, and Glu507, Gly508, and Gly509 (in helix α18) in the C-terminal part of the adjacent monomer (Fig. S5 in the Supplementary Material). On the other hand, a water molecule was observed in this position in the E-XMP* structure (and this region was not visible in our apo structure). This K^+ binding site is observed in other crystal structures and has been proposed to act as a ball-and-socket joint that facilitates the conformational changes required for completion of the catalytic cycle (Riera et al. 2011).

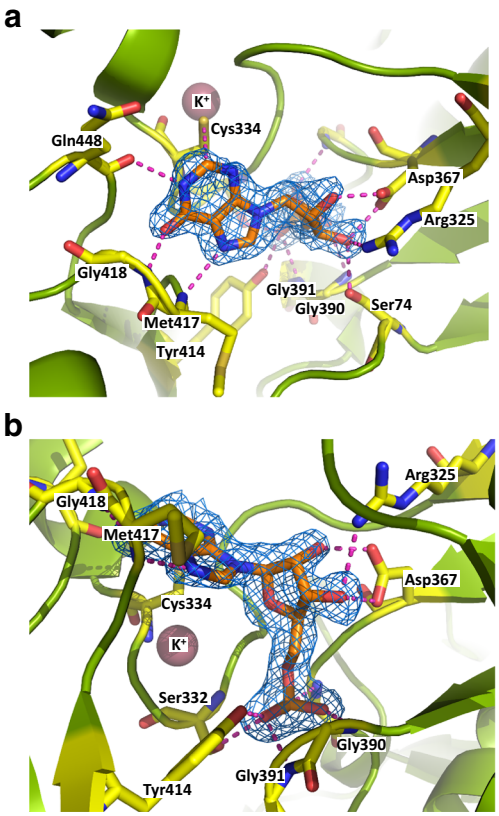

Fig. 6 View of the active site of AgIMPDH with IMP and K^+ ion bound. Two different views (**a** and **b**) of the protein (chain **B** in the asymmetric unit) is represented in *green cartoons*. The residues involved in hydrogen bonding with IMP are labeled and shown as *yellow* (C), *red* (O), *brown* (S), and *blue* (N) sticks. IMP is represented in *orange* (C), *blue* (N), and *red* (O and P) sticks. The K^+ ion is represented as a *pink sphere*. Hydrogen bonds between IMP and protein residues are represented as *magenta-dashed lines*. The *blue* mesh around IMP represents the simulated annealing omit $2mF_o$-DF_c electron density map contoured at 1 σ level. The figures have been generated using PyMOL (The PyMOL Molecular Graphics System, Schrödinger, LLC)

IMPDH activity significantly influences metabolite production in *A. gossypii*

We next attempted to characterize the effects of the manipulation of AgIMPDH's activity on the production of metabolites of biotechnological interest in *A. gossypii*. For this purpose, we performed a side-by-side comparison of the wild-type and the mutant strains Δ*IMPDH* and *P-$_{GPD}$-IMPDH*, which have been described above. We initially focused on the production of riboflavin, given that *Ashbya* is the main industrial producer of this important vitamin (Kato and Park 2012). Additionally, we also studied the production of the nucleosides guanosine and inosine, given their interest as precursors of the foodstuff additives IMP and GMP with flavoring, nutritional and pharmaceutical properties (Ledesma-Amaro et al. 2013). To this respect, we have recently shown that both nucleosides are excreted to the extracellular media of *A. gossypii*'s flask fermentations at milligrams-per-liter levels and have proposed this fungus as a promising candidate for nucleoside industrial production (Ledesma-Amaro et al. 2015). Given that overexpression of IMPDH causes the disruption of the *STE12* locus (by the insertion of the *P-$_{GPD}$-IMPDH* construct), we previously demonstrated that the disruption of *STE12* does not affect inosine, guanosine, riboflavin production, or growth rate (Table S2 in the Supplementary Material).

As shown in Fig. 7 (and Table S2 in the Supplementary Material), *IMPDH* depletion resulted in a significant 20-fold increase in the production of inosine as well as a decrease in guanosine and riboflavin levels. It also seriously

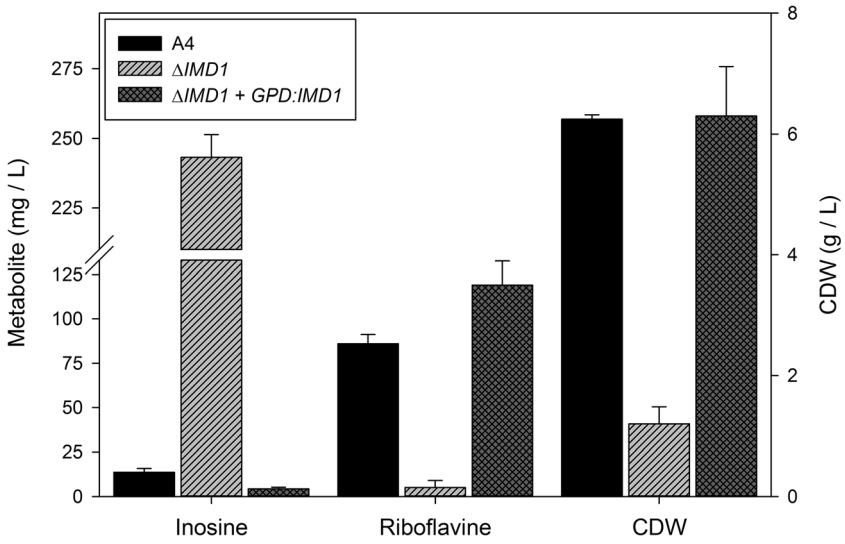

Fig. 7 Effects of the manipulation of IMPDH on the production of metabolites in *A. gossypii*. The graph shows the extracellular inosine/guanosine and total (intracellular + extracellular) riboflavin concentration, as well as the cell dry weight of the *A. gossypii* strains engineered in this study. Cultures were grown for 5 days in flasks containing MA2. *Error bars* represent the standard deviations of three independent experiments

compromised cell growth in rich MA2 media, as demonstrated by a 6-fold reduction of biomass. On the other hand, *IMPDH* overexpression significantly decreased inosine excretion, while the guanosine levels remained constant compared to the wild type strain. Remarkably, *IMPDH* overexpression enhanced about 40 % riboflavin production (Fig. 7 and Table S2 in Supplementary Material), a result with obvious industrial implications.

Discussion

The modification of the biosynthetic pathways to enhance the production of a particular metabolite through the redirection of the cellular metabolic flux is one of the main objectives of biotechnology. The metabolic manipulation of the fungus *A. gossypii* to improve riboflavin production is a very representative and successful example which is widely used at present in food industry. We have previously reported that the manipulation of the enzymes PRPP synthetase (Jiménez et al. 2008) and PRPP amidotransferase (Jiménez et al. 2005) increased the metabolic flux through the de novo purine nucleotide pathway, the GTP availability, and the subsequent riboflavin production. Following these reports, we decided to characterize *A. gossypii* IMP dehydrogenase, the enzyme that catalyzes the limiting step of guanine nucleotide biosynthesis from the de novo synthetized IMP (Fig. 1), and test the effects of its manipulation on cell growth and metabolite production.

The genome of *A. gossypii* contains only one gene encoding for IMPDH activity. A phylogenetic analysis of IMPDH proteins from prokaryotic and eukaryotic organisms showed, as expected, strong similarities to other yeast and fungi IMPDHs (the closest ortholog is *S. cerevisiae* IMD4) and revealed that AgIMPDH is evolutionarily closed to the two human isoforms. These findings suggest that the fungal and human enzymes evolved from a common ancestor that might be different from the one that gave rise to the bacterial and protozoan IMPDHs. This hypothesis is further supported by the fact that AgIMPDH is highly sensitive to MPA and shows micromolar affinity for—and is inhibited by—its substrate NAD^+, common to mammalian but distinct from bacterial IMPDHs, which show millimolar NAD^+ affinities and do not present substrate inhibition (Hedstrom 2009). To this respect, AgIMPDH possess the previously described sequence signatures associated with eukaryotic IMPDH enzymes that differentiate them from the bacterial ones (Zhang et al. 1999a). Interestingly, the first N-terminal residues, which in AgIMPDH comprise two short 3_{10} and two alpha helices (Fig. S1 in the Supplementary Material), contact the catalytic domain of the adjacent monomer, contributing to the stabilization of the tetramer (Figs. 5a, b). A similar interaction is also observed in the crystal structure of the IMPDH from the encapsulated yeast *Cryptococcus neoformans* (PDB code 4AF0; (Morrow et al. 2012)), and according to our multiple protein sequence alignments (Fig. S1 in the Supplementary Material) and the structures available at the PDB for other 15 different species, it might represent a specific signature of fungal IMPDHs.

The enzyme kinetics in vitro showed a typical Michaelis-Menten behavior with K_M values similar to those reported for the non-flavinogenic-related organism *S. cerevisiae* (McPhillips et al. 2004; Jenks and Reines 2005). These data indicate that the efficiency of AgIMPDH itself is not a limiting factor to support the high—naturally occurring—levels of metabolic flux through the guanine nucleotide pathway in *A. gossypii*.

AgIMPDH is inhibited by the reaction product XMP in a competitive manner. Remarkably, XMP and IMP affinity for AgIMPDH lie within the same concentration range (mid-micromolar range), indicating that the XMP feedback inhibition

significantly contribute to the regulation of the cellular guanine nucleotide pool in *A. gossypii*. In fact, we have recently found that GMP, the classical competitive inhibitor of IMPDH (Gilbert et al. 1979) has a K_i in the order of 0.5 mM (Buey et al.; submitted manuscript), well above the physiological intracellular concentration, estimated in about 60 μM (Traut 1994). Therefore, these data challenge the physiological role of GMP in IMPDH inhibition. Physiological GMP inhibition has been also questioned for the *E. coli* enzyme (Pimkin and Markham 2008). Moreover, we have recently determined that, in the wild-type *A. gossypii A4* strain, the intracellular concentrations of XMP are about 8 times higher than those of GMP and about 40 times larger than IMP (Ledesma-Amaro et al. 2015), further supporting the hypothesis that XMP—rather than GMP—feedback inhibition might be a main regulator of IMPDH activity in vivo. Therefore, by solving the high-resolution crystallographic structures in complex with IMP and XMP, we have settled a reliable basis for computational modeling as well as protein engineering strategies towards enzyme optimization and/or product inhibition removal which we are at present developing in our laboratory.

Our in vivo experiments demonstrated that the gene *IMPDH* is essential for *A. gossypii* viability and its disruption resulted in auxotrophy for guanine and strongly reduced growth rates in rich media. In fact, the strain *ΔIMPDH* produced only residual amounts of riboflavin, due to the reduction in the metabolic flux through the de novo guanine nucleotide biosynthetic pathway, which results in a complete dependence on the salvage pathway for guanine nucleotide synthesis. The blockage in the guanine nucleotide pathway increases IMP availability that, in turn, is converted to inosine and subsequently excreted to the culture media (Ledesma-Amaro et al. 2015). Indeed, the *ΔIMPDH* strain excreted 20 times more inosine per liter of culture (and as much as 100 times more per gram of cell dry weight; Table S2 in the Supplementary Material) than the wild-type strain. Inosine is a biotechnologically interesting molecule since it is used in food industry as the direct precursor of IMP, a flavor enhancer with health beneficial effects, related to their antioxidant, neuroprotective, cardiotonic, and immunomodulatory properties (Ledesma-Amaro et al. 2013). Therefore, the *ΔIMPDH* strain is a promising candidate for further optimization and use in nucleoside production at industrial level.

On the other hand, the strain that overexpresses AgIMPDH, P_{GPD}-*IMPDH*, recovered prototrophy for guanine and redirected the metabolic flux through the purine pathway. The fact that this strain does not excrete higher levels of guanosine than the wild type might indicate that the excess of metabolic flux through the GTP pathway is mostly derived to riboflavin production. Indeed, this strain produced 40 % more riboflavin than the wild-type strain. This finding clearly represents a significant improvement in terms of industrial production and shows a relevant advance that might be subjected to further manipulations. Moreover, we envisage that such redirection of the metabolic flux towards guanine nucleotide production will be also a useful tool to improve the production of other guanine nucleotide derived metabolites, such as folates (vitamin B9).

In conclusion, in the present study, we have exhaustively characterized biochemically, structurally, and functionally the enzyme IMP dehydrogenase from *A. gossypii*. The obtained results pave the way for further enzyme optimization by removing product inhibition following protein engineering approaches. They further demonstrate that the genetic manipulation of this enzyme significantly influences the production of metabolites of biotechnological interest. Altogether, the results reported in this manuscript significantly contribute to the metabolic engineering toolbox that our laboratory, and others, is developing to improve the production of metabolites with biotechnological interest in *A. gossypii*.

Acknowledgments This work was supported by grant BIO2014-56930-P from the Spanish Ministerio de Economía y Competitividad. Rubén M Buey is supported by a "Ramón y Cajal" contract from the Spanish Ministerio de Economía y Competitividad and by a Marie Curie Career Integration Grant (EB-SxIP; FP7-PEOPLE-2011-CIG-293831). We thank MD. Sánchez and S. Domínguez for excellent technical help and N. Skinner for correcting the manuscript. X-ray crystallography data were collected at BL13 (XALOC) beamline at ALBA Synchrotron Light Facility with the collaboration of ALBA staff.

Conflict of interest RMB, RLA, and JLR declare conflict of interest due to issued and outstanding patent applications covering aspects of this work.

References

Adams PD, Afonine PV, Bunkoczi G, Chen VB, Davis IW, Echols N, Headd JJ, Hung LW, Kapral GJ, Grosse-Kunstleve RW, McCoy AJ, Moriarty NW, Oeffner R, Read RJ, Richardson DC, Richardson JS, Terwilliger TC, Zwart PH (2010) PHENIX: a comprehensive python-based system for macromolecular structure solution. Acta Crystallogr D Biol Crystallogr 66(Pt 2):213–221. doi:10.1107/S0907444909052925

Allison AC, Eugui EM (2000) Mycophenolate mofetil and its mechanisms of action. Immunopharmacology 47(2–3):85–118

Alonso-García N, Inglés-Prieto A, Sonnenberg A, de Pereda JM (2009) Structure of the calx-β domain of the integrin β4 subunit: insights into function and cation-independent stability. Acta Crystallogr D Biol Crystallogr 65(Pt 8):858–871. doi:10.1107/S0907444909018745

Bacher A, Eberhardt S, Richter G (1996) Biosynthesis of riboflavin. In: Neidhardt FC, Curtiss III R, Ingraham JL, Lin ECC, Low KB, Magasanik B, Reznikoff WS, Riley M, Schaechter M, Umbarger HE (eds) *Escherichia coli* and *Salmonella*: cellular and molecular biology. ASM Press, Washington DC, pp. 657–664

Bacher A, Eberhardt S, Fischer M, Kis K, Richter G (2000) Biosynthesis of vitamin B2 (riboflavin). Annu Rev Nutr 20:153–167. doi:10.1146/annurev.nutr.20.1.153

Bateman A (1997) The structure of a domain common to archaebacteria and the homocystinuria disease protein. Trends Biochem Sci 22(1):12–13

Benson DA, Clark K, Karsch-Mizrachi I, Lipman DJ, Ostell J, Sayers EW (2014) GenBank. Nucleic Acids Res 42(Database issue):D32–D37. doi:10.1093/nar/gkt1030

Braun-Sand SB, Peetz M (2010) Inosine monophosphate dehydrogenase as a target for antiviral, anticancer, antimicrobial and immunosuppressive therapeutics. Future Med Chem 2(1):81–92. doi:10.4155/fmc.09.147

Castresana J (2000) Selection of conserved blocks from multiple alignments for their use in phylogenetic analysis. Mol Biol Evol 17(4): 540–552

Chong CR, Qian DZ, Pan F, Wei Y, Pili R, Sullivan Jr DJ, Liu JO (2006) Identification of type 1 inosine monophosphate dehydrogenase as an antiangiogenic drug target. J Med Chem 49(9):2677–2680. doi:10.1021/jm051225t

Cossins EA, Chen L (1997) Folates and one-carbon metabolism in plants and fungi. Phytochemistry 45(3):437–452

Dietrich FS, Voegeli S, Brachat S, Lerch A, Gates K, Steiner S, Mohr C, Pohlmann R, Luedi P, Choi S, Wing RA, Flavier A, Gaffney TD, Philippsen P (2004) The *Ashbya gossypii* genome as a tool for mapping the ancient *Saccharomyces cerevisiae* genome. Science 304(5668):304–307. doi:10.1126/science.1095781

Dobie F, Berg A, Boitz J, Jardim A (2007) Kinetic characterization of inosine monophosphate dehydrogenase of *Leishmania donovani*. Mol Biochem Parasitol 152(1):11–21. doi:10.1016/j.molbiopara.2006.11.007

Emsley P, Lohkamp B, Scott WG, Cowtan K (2010) Features and development of Coot. Acta Crystallogr D Biol Crystallogr 66(Pt 4):486–501. doi:10.1107/S0907444910007493

Forster C, Santos MA, Ruffert S, Kramer R, Revuelta JL (1999) Physiological consequence of disruption of the VMA1 gene in the riboflavin overproducer *Ashbya gossypii*. J Biol Chem 274(14): 9442–9448

Gan L, Seyedsayamdost M, Shuto S, Matsuda A, Petsko G, Hedstrom L (2003) The immunosuppressive agent mizoribine monophosphate forms a transition state analogue complex with inosine monophosphate dehydrogenase. Biochemistry 42(4):857–863. doi:10.1021/bi0271401

Gattiker A, Rischatsch R, Demougin P, Voegeli S, Dietrich FS, Philippsen P, Primig M (2007) *Ashbya* Genome Database 3.0: a cross-species genome and transcriptome browser for yeast biologists. BMC Genomics 8:9. doi:10.1186/1471-2164-8-9

Gilbert H, Lowe C, Drabble W (1979) Inosine 5′-monophosphate dehydrogenase of *Escherichia coli*. Purification by affinity chromatography, subunit structure and inhibition by guanosine 5′-monophosphate. Biochem J 183(3):481–494

Gross SS, Levi R (1992) Tetrahydrobiopterin synthesis. An absolute requirement for cytokine-induced nitric oxide generation by vascular smooth muscle. J Biol Chem 267(36):25722–25729

Hedstrom L (2009) IMP dehydrogenase: structure, mechanism, and inhibition. Chem Rev 109(7):2903–2928. doi:10.1021/cr900021w

Hedstrom L, Liechti G, Goldberg JB, Gollapalli DR (2011) The antibiotic potential of prokaryotic IMP dehydrogenase inhibitors. Curr Med Chem 18(13):1909–1918

Hyle J, Shaw R, Reines D (2003) Functional distinctions between IMP dehydrogenase genes in providing mycophenolate resistance and guanine prototrophy to yeast. J Biol Chem 278(31):28470–28478. doi:10.1074/jbc.M303736200

Jaroszewski L, Li Z, Cai XH, Weber C, Godzik A (2011) FFAS server: novel features and applications. Nucleic Acids Res 39 (Web Server issue):W38-44 doi:10.1093/nar/gkr441

Jenks MH, Reines D (2005) Dissection of the molecular basis of mycophenolate resistance in *Saccharomyces cerevisiae*. Yeast 22(15): 1181–1190. doi:10.1002/yea.1300

Jiménez A, Santos MA, Pompejus M, Revuelta JL (2005) Metabolic engineering of the purine pathway for riboflavin production in *Ashbya gossypii*. Appl Environ Microbiol 71(10):5743–5751. doi:10.1128/AEM.71.10.5743-5751.2005

Jiménez A, Santos MA, Revuelta JL (2008) Phosphoribosyl pyrophosphate synthetase activity affects growth and riboflavin production in *Ashbya gossypii*. BMC Biotechnol 8:67. doi:10.1186/1472-6750-8-67

Juanhuix J, Gil-Ortiz F, Cuni G, Colldelram C, Nicolas J, Lidon J, Boter E, Ruget C, Ferrer S, Benach J (2014) Developments in optics and performance at BL13-XALOC, the macromolecular crystallography beamline at the ALBA synchrotron. J Synchrotron Radiat 21(Pt 4): 679–689. doi:10.1107/S160057751400825X

Kabsch W (2010) Xds. Acta Crystallogr D Biol Crystallogr 66(Pt 2):125–132. doi:10.1107/S0907444909047337

Kato T, Park E (2012) Riboflavin production by *Ashbya gossypii*. Biotechnol Lett 34(4):611–618. doi:10.1007/s10529-011-0833-z

Larkin MA, Blackshields G, Brown NP, Chenna R, McGettigan PA, McWilliam H, Valentin F, Wallace IM, Wilm A, Lopez R, Thompson JD, Gibson TJ, Higgins DG (2007) Clustal W and Clustal X version 2.0. Bioinformatics 23(21):2947–2948. doi:10.1093/bioinformatics/btm404

Ledesma-Amaro R, Jiménez A, Santos MA, Revuelta JL (2013) Biotechnological production of feed nucleotides by microbial strain improvement. Process Biochem 48:7

Ledesma-Amaro R, Santos MA, Jiménez A, Revuelta JL (2014a) Strain design of *Ashbya gossypii* for single-cell oil production. Appl Environ Microbiol 80(4):1237–1244. doi:10.1128/AEM.03560-13

Ledesma-Amaro R, Santos MA, Jiménez A, Revuelta JL (2014b) Tuning single-cell oil production in *Ashbya gossypii* by engineering the elongation and desaturation systems. Biotechnol Bioeng 111(9): 1782–1791. doi:10.1002/bit.25245

Ledesma-Amaro R, Buey RM, Revuelta JL (2015) Increased production of inosine and guanosine by means of metabolic engineering of the purine pathway in *Ashbya gossypii*. Microb Cell Fact 14:58. doi:10.1186/s12934-015-0234-4

Long H, Cameron S, Yu L, Rao Y (2006) De novo GMP synthesis is required for axon guidance in *Drosophila*. Genetics 172(3):1633–1642. doi:10.1534/genetics.105.042911

Makowska-Grzyska M, Kim Y, Wu R, Wilton R, Gollapalli D, Wang X, Zhang R, Jedrzejczak R, Mack J, Maltseva N, Mulligan R, Binkowski T, Gornicki P, Kuhn M, Anderson W, Hedstrom L, Joachimiak A (2012) *Bacillus anthracis* inosine 5′-monophosphate dehydrogenase in action: the first bacterial series of structures of phosphate ion-, substrate-, and product-bound complexes. Biochemistry 51(31):6148–6163. doi:10.1021/bi300511w

McCoy AJ, Grosse-Kunstleve RW, Adams PD, Winn MD, Storoni LC, Read RJ (2007) Phaser crystallographic software. J Appl Crystallogr 40(Pt 4):658–674. doi:10.1107/S0021889807021206

McPhillips C, Hyle J, Reines D (2004) Detection of the mycophenolate-inhibited form of IMP dehydrogenase in vivo. Proc Natl Acad Sci U S A 101(33):12171–12176. doi:10.1073/pnas.0403341101

Morrow CA, Valkov E, Stamp A, Chow EW, Lee IR, Wronski A, Williams SJ, Hill JM, Djordjevic JT, Kappler U, Kobe B, Fraser JA (2012) De novo GTP biosynthesis is critical for virulence of the fungal pathogen *Cryptococcus neoformans*. PLoS Pathog 8(10):e1002957 doi:10.1371/journal.ppat.1002957

Murray AW (1971) The biological significance of purine salvage. Annu Rev Biochem 40:811–826. doi:10.1146/annurev.bi.40.070171.004115

Nagano N, Orengo CA, Thornton JM (2002) One fold with many functions: the evolutionary relationships between TIM barrel families based on their sequences, structures and functions. J Mol Biol 321(5):741–765

Nair V, Shu Q (2007) Inosine monophosphate dehydrogenase as a probe in antiviral drug discovery. Antivir Chem Chemother 18(5):245–258

Page RD (1996) TreeView: an application to display phylogenetic trees on personal computers. Comput Appl Biosci 12(4):357–358

Park EY, Ito Y, Nariyama M, Sugimoto T, Lies D, Kato T (2011) The improvement of riboflavin production in *Ashbya gossypii* via disparity mutagenesis and DNA microarray analysis. Appl Microbiol Biotechnol 91(5):1315–1326. doi:10.1007/s00253-011-3325-0

Pimkin M, Markham G (2008) The CBS subdomain of inosine 5′-monophosphate dehydrogenase regulates purine nucleotide turnover. Mol Microbiol 68(2):342–359. doi:10.1111/j.1365-2958.2008.06153.x

Potterton E, Briggs P, Turkenburg M, Dodson E (2003) A graphical user interface to the CCP4 program suite. Acta Crystallogr D Biol Crystallogr 59(Pt 7):1131–1137

Prosise GL, Wu JZ, Luecke H (2002) Crystal structure of *Tritrichomonas foetus* inosine monophosphate dehydrogenase in complex with the inhibitor ribavirin monophosphate reveals a catalysis-dependent ion-binding site. J Biol Chem 277(52):50654-50659 doi:10.1074/jbc.M208330200

Rao V, Shepherd S, Owen R, Hunter W (2013) Structure of *Pseudomonas aeruginosa* inosine 5′-monophosphate dehydrogenase. Acta Crystallogr Sect F Struct Biol Cryst Commun 69(Pt 3):243–247. doi:10.1107/s1744309113002352

Ratcliffe AJ (2006) Inosine 5′-monophosphate dehydrogenase inhibitors for the treatment of autoimmune diseases. Curr Opin Drug Discov Devel 9(5):595–605

Revuelta JL, Buitrago MJ, Santos MA (1998) Riboflavin biosynthesis in fungi. Patent nr WO9526406 In., C12N15/52(edn: BASF AG (DE))

Riera TV, Zheng L, Josephine HR, Min D, Yang W, Hedstrom L (2011) Allosteric activation via kinetic control: potassium accelerates a conformational change in IMP dehydrogenase. Biochemistry 50(39):8508–8518. doi:10.1021/bi200785s

Stahmann K, Revuelta J, Seulberger H (2000) Three biotechnical processes using *Ashbya gossypii*, *Candida famata*, or *Bacillus subtilis* compete with chemical riboflavin production. Appl Microbiol Biotechnol 53(5):509-516 doi:10.1007/s002530051649

Thompson JD, Gibson TJ, Higgins DG (2002) Multiple sequence alignment using ClustalW and ClustalX. Curr Protoc Bioinformatics Chapter 2:Unit 2.3 doi:10.1002/0471250953.bi0203s00

Traut TW (1994) Physiological concentrations of purines and pyrimidines. Mol Cell Biochem 140(1):1-22

Trzhtsinskaya BV, Abramova ND (1991) Imidazole-2-thiones: synthesis, structure and properties. Sulfur Reports 10:389–421

Umejiego NN, Gollapalli D, Sharling L, Volftsun A, Lu J, Benjamin NN, Stroupe AH, Riera TV, Striepen B, Hedstrom L (2008) Targeting a prokaryotic protein in a eukaryotic pathogen: identification of lead compounds against cryptosporidiosis. Chem Biol 15(1):70–77. doi:10.1016/j.chembiol.2007.12.010

Vandamme EJ (1992) Production of vitamins, coenzymes and related biochemicals by biotechnological processes. J Chem Technol Biotechnol 53(4):313–327

Wasserstrom L, Lengeler KB, Walther A, Wendland J (2013) Molecular determinants of sporulation in *Ashbya gossypii*. Genetics 195(1):87–99. doi:10.1534/genetics.113.151019

Wendland J, Ayad-Durieux Y, Knechtle P, Rebischung C, Philippsen P (2000) PCR-based gene targeting in the filamentous fungus *Ashbya gossypii*. Gene 242(1–2):381–391

Wendland J, Dunkler A, Walther A (2011) Characterization of α-factor pheromone and pheromone receptor genes of *Ashbya gossypii*. FEMS Yeast Res 11(5):418–429. doi:10.1111/j.1567-1364.2011.00732.x

Winn MD, Isupov MN, Murshudov GN (2001) Use of TLS parameters to model anisotropic displacements in macromolecular refinement. Acta Crystallogr D Biol Crystallogr 57(Pt 1):122–133

Zalkin H, Dixon JE (1992) De novo purine nucleotide biosynthesis. Prog Nucleic Acid Res Mol Biol 42:259–287

Zhang R, Evans G, Rotella F, Westbrook E, Huberman E, Joachimiak A, Collart FR (1999a) Differential signatures of bacterial and mammalian IMP dehydrogenase enzymes. Curr Med Chem 6(7):537–543

Zhang R, Evans G, Rotella FJ, Westbrook EM, Beno D, Huberman E, Joachimiak A, Collart FR (1999b) Characteristics and crystal structure of bacterial inosine-5′-monophosphate dehydrogenase. Biochemistry 38(15):4691–4700. doi:10.1021/bi982858v